ChemPubSoc Europe

DOI: 10.1002/open.201800282

Open Access ChemistryOPEN Full Papers

A Series of Analogues to the AT_2R Prototype Antagonist C38 Allow Fine Tuning of the Previously Reported Antagonist Binding Mode

Rebecka Isaksson,[a] Jens Lindman,[a] Johan Wannberg,[b] Jessica Sallander,[c] Maria Backlund,[d] Dhaniel Baraldi,[e] Robert Widdop,[e] Mathias Hallberg,[f] Johan Åqvist,[c] Hugo Gutierrez de Teran,[c] Johan Gising,[a] and Mats Larhed*[a]

We here report on our continued studies of ligands binding to the promising drug target angiotensin II type 2 receptor (AT_2R). Two series of compounds were synthesized and investigated. The first series explored the effects of adding small substituents to the phenyl ring of the known selective nonpeptide AT_2R antagonist **C38**, generating small but significant shifts in AT_2R affinity. One compound in the first series was equipotent to **C38** and showed similar kinetic solubility, and stability in both human and mouse liver microsomes. The second series was comprised of new bicyclic derivatives, amongst which one ligand exhibited a five-fold improved affinity to AT_2R as compared to **C38**. The majority of the compounds in the second series, including the most potent ligand, were inferior to **C38** with regard to stability in both human and mouse microsomes. In contrast to our previously reported findings, ligands with shorter carbamate alkyl chains only demonstrated slightly improved stability in microsomes. Based on data presented herein, a more adequate, tentative model of the binding modes of ligand analogues to the prototype AT_2R antagonist **C38** is proposed, as deduced from docking redefined by molecular dynamic simulations.

1. Introduction

The renin-angiotensin-aldosterone system (RAAS) is well-known for its role in fluid-electrolyte control and blood-pressure regulation; there are several drugs on the market for the treatment of hypertension targeting proteins in RAAS. Although a series of bioactive components are formed in RAAS, the octapeptide angiotensin II (AngII) is considered to constitute the major effector peptide.[1] Hence, inhibitors of the two

[a] R. Isaksson, J. Lindman, Dr. J. Gising, Prof. Dr. M. Larhed
Department of Medicinal Chemistry
Uppsala University
SE-751 23, Uppsala, SWEDEN
E-mail: mats.larhed@ilk.uu.se
[b] Dr. J. Wannberg
SciLifeLab Drug Discovery & Development Platform, Medicinal Chemistry – Lead Identification, Department of Medicinal Chemistry
Uppsala University
SE-751 23, Uppsala, SWEDEN
[c] Dr. J. Sallander, Prof. Dr. J. Åqvist, Dr. H. Gutierrez de Teran
Department of Cell and Molecular Biology
Uppsala University
SE-751 23, Uppsala, SWEDEN
[d] Dr. M. Backlund
SciLifeLab Drug Discovery & Development Platform, ADME of Therapeutics, Department of Pharmacy
Uppsala University
SE-751 23 Uppsala, SWEDEN
[e] Dr. D. Baraldi, Prof. Dr. R. Widdop
Department of Pharmacology
Monash University
Clayton, Victoria, 3800 AUSTRALIA
[f] Prof. Dr. M. Hallberg
The Beijer Laboratory, Department of Pharmaceutical Biosciences
Uppsala University
SE-751 24, Uppsala, SWEDEN

Supporting information for this article is available on the WWW under https://doi.org/10.1002/open.201800282

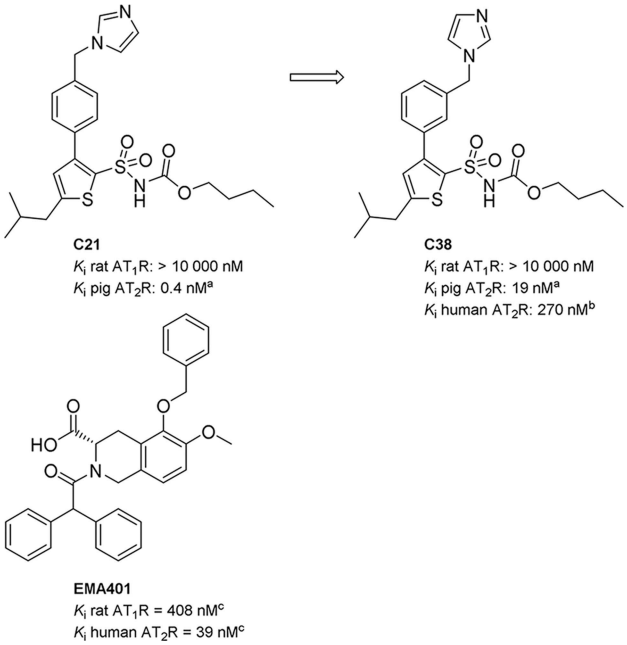

Figure 1. The first selective nonpeptide AT_2R agonist **C21**, the structurally related AT_2R antagonist **C38**, and the AT_2R antagonist **EMA401**. [a] AT_2R from pig uterus membrane assay. [b] HEK-293 cells expressing human AT_2R. [c] See Ref. [19].

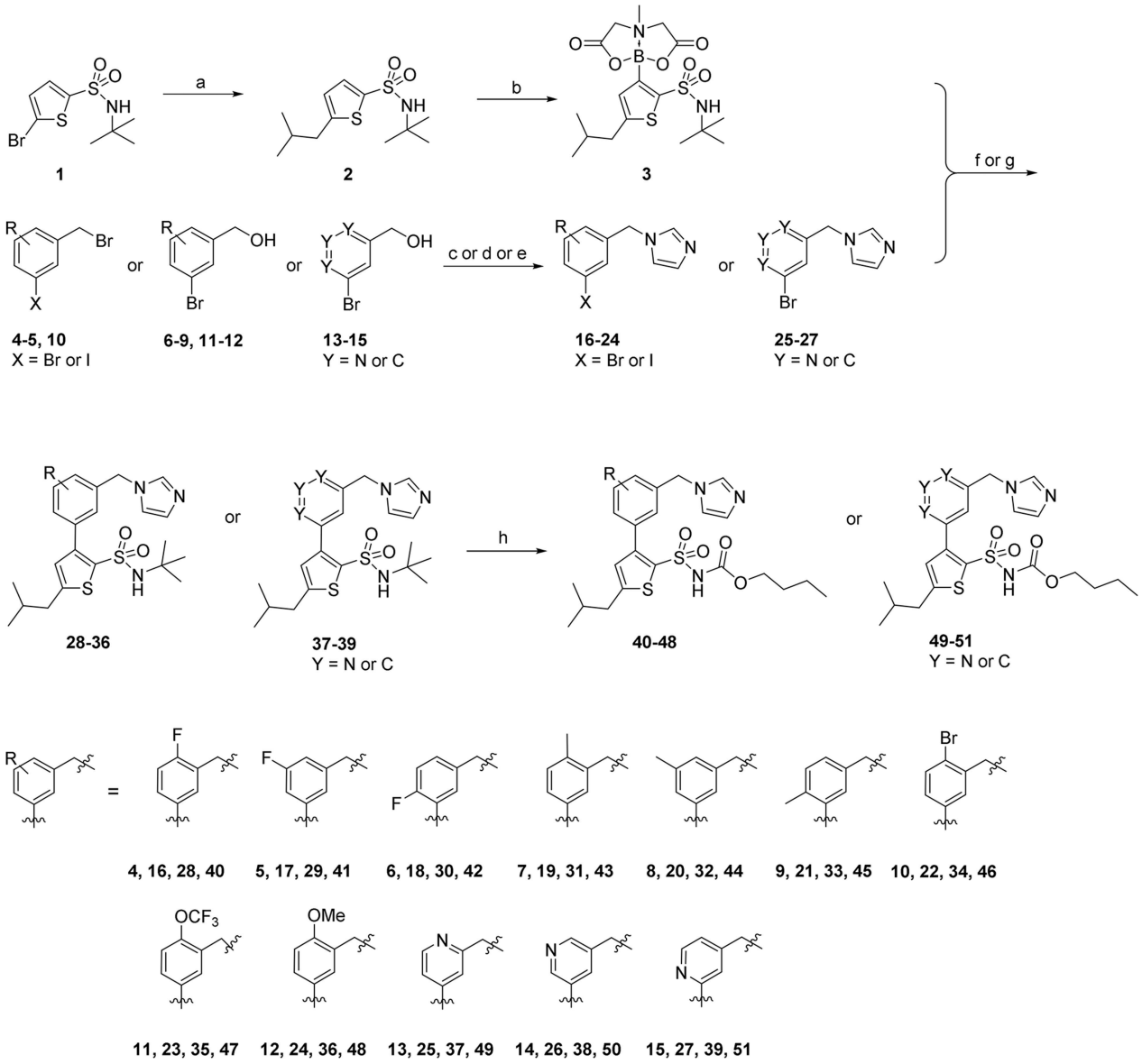

Scheme 1. Synthesis of AT_2R ligands **40**–**51**. a) $ZnCl_2$, isobutylmagnesium chloride, Pd(*t*-$Bu_3P)_2$, toluene, THF; b) 1. *n*-BuLi (4.5 eq.), triisopropyl borate, THF; 2. methyliminodiacetic acid, DMSO, toluene; c) imidazole, DCM (to **16**–**17**) ; d) 1. TEA, MsCl, DCM; 2. imidazole, DMF (to **18**–**19**, **22**–**23**, **25**–**27**); e) 1. thionyl chloride, DCM; 2. imidazole DMF (to **20**–**21**, **24**); f) $PdCl_2$(dppf), K_2CO_3, DME, H_2O (to **28**–**33**, **35**–**39**); g) $Pd(PPh_3)_4$, K_2CO_3, EtOH, H_2O, THF (to **34**); h) 1. TFA; 2. butyl chloroformate, Na_2CO_3, DCM, H_2O.

proteases important for formation of AngII (angiotensin converting enzyme, ACE, and renin) or compounds acting as antagonists at its receptor (i.e. the sartans) are well established therapeutics. The angiotensin II type 1 receptor (AT_1R) was long believed to be the only mediator of the effects elicited by the endogenous AngII. However, in the late 1980s the first evidence of a second protein binding AngII appeared in the literature, the angiotensin II type 2 receptor (AT_2R).[2,3] This receptor proved to be an enigmatic protein, which in recent years has emerged as a promising new drug target.[4–6]

AT_2R is predominantly expressed in fetal tissue, indicating its important role in fetal development.[7,8] In adults AT_2R is mainly expressed in uterus, adrenal gland, smooth muscle, heart, and kidney.[9,10] Notably, AT_2R is strongly upregulated following tissue damage,[11,12] such as vascular[13] and neuronal injury,[14] myocardial infarction[15–17] and brain ischemia.[18]

There are currently two AT_2R ligands in clinical trials, for different indications, again raising questions regarding the role (s) of this protein. The AT_2R antagonist **EMA401** (Figure 1), acquired by Novartis from Spinifex Pharmaceuticals Pty Ltd, Australia, is in phase II clinical trials for peripheral neuropathic pain.[19,20] The AT_2R agonist **C21** (Figure 1), developed in our laboratory,[21] is entering phase II clinical trials as a potential treatment for idiopathic pulmonary fibrosis. Recently published reviews detail the discovery of **C21**,[22,23] and a large number of structurally related AT_2R ligands were subsequently disclosed.[24–28] In 2012 we reported that shifting the imidazole head group from the para position in the agonist **C21** to meta

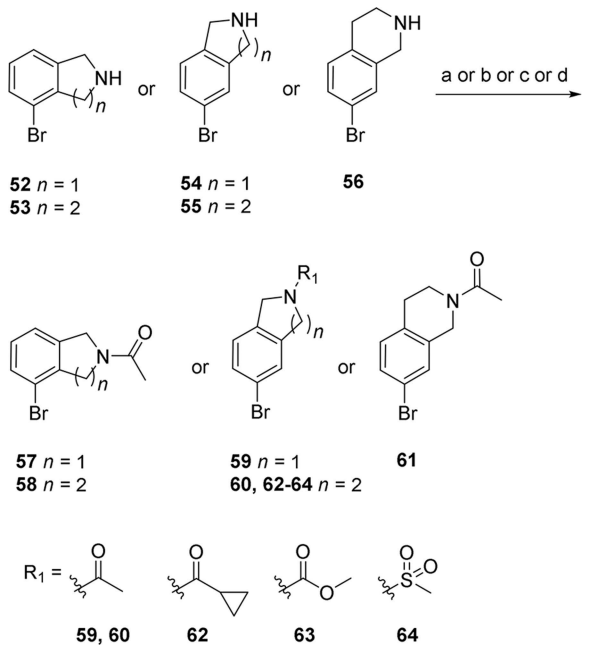

Scheme 2. Synthesis of compounds **57**–**64**. a) Acetic anhydride, K_2CO_3, MeCN (to **57**–**61**); b) cyclopropanecarbonyl chloride, DIPEA, DCM (to **62**); c) methyl chloroformate, DIPEA, DCM (to **63**); d) MsCl, DIPEA, DCM (to **64**).

position switches the pharmacological profile, resulting in the prototype antagonist **C38** (Figure 1).[29,30]

The first crystal structure of AT_1R binding antagonist ZD7155 was published in 2015 by Zhang et al., enabling further elucidation of the binding mode of AT_1R ligands.[31,32] The crystal structure allowed for comparison with our predicted inactive-like homology model of both AT_1R and AT_2R, confirming the general topology and residue location in the binding cavity of our models. Minor structural changes resulting in an altered pharmacological profile. which could be rationalized in our AT_2R homology model.[33] Zhang et al. recently published the crystal structure of AT_2R binding the selective AT_2R antagonist L-161,638, revealing a similar binding mode in comparison to ZD7155 from the previously published AT_1R crystal structure.[34] The published structures of both AT_1R and AT_2R provide insight in the structure-function relationship and allows design of new selective ligands.

We herein report the impact on AT_2R affinity of chemical modifications of the prototype AT_2R antagonist **C38**, and consequently adjust our previously reported AT_2 receptor-antagonist model to the new SAR data through computational simulations using the newly published AT_2R crystal structure.[34]

2. Results and Discussion

2.1. Chemistry

Two series of compounds were synthesized: the first series was motivated by our ambition to explore the impact of adding substituents to the central phenyl ring of the **C38** core structure, as well as if replacing the phenyl for pyridine could improve solubility. In the second series we explored a new head group of **C38** where the benzyl imidazole moiety was exchanged for bicyclic amides. Previous work from our group demonstrated that the affinity and selectivity of the ligands can be retained by replacing the imidazole with amides;[29] with these new bicyclic amides we continue our exploration of the promising amide functionality by trying to ascertain the binding conformation. A majority of the bicyclic compounds retained a shortened sulfonyl carbamate chain, as we have recently found this to be beneficial for metabolic stability.[35] The key building block for the synthesis of both series was MIDA boronate **3**, that was synthesized according to the pathway previously published by our group.[35] Microwave assisted Negishi coupling in a sealed vial of 5-bromo-*N*-(*tert*-butyl)thiophene-2-sulfonamide (**1**)] with in situ generated isobutylzinc chloride produced *N*-(*tert*-butyl)-5-isobutylthiophene-2-sulfonamide (**2**) in 51% yield.[36,37] Compound **2** was in turn converted to the MIDA boronate (**3**) in 76% yield over 2 steps (Scheme 1). Substituted benzylimidazoles and pyridinemethyl imidazoles **16–27** were generated either via direct alkylation of 3-halo benzylbromides (**4**–**5**, **10**) with imidazole, or via chlorination or mesylation of the 3-bromo benzylalcohols (**6**–**9**, **11**–**15**) and subsequent alkylation with imidazole. Chlorination was initially tested for 3-bromo benzylalcohols **6**, **7**, and **11**, however generated no or low yields. Mesylation was instead explored and yielded the desired products **18**, **19**, and **23** in moderate to good yields (72%, 43%, and 66% respectively). Once generated, the benzyl-/pyridine-methyl imidazoles (**16-27**) were coupled with the MIDA boronate **3** under Suzuki conditions in sealed vials either using conventional heating (**16**–**18**) or microwave assisted (**19**–**27**), delivering the *tert*-butyl protected sulfonamides **28**–**39**.[36,37] A *tert*-butyl deprotection followed by treatment with butyl chloroformate resulted in the target compounds **40**–**51**, generated in low to fair yields over 3 steps (3-28%). The low yields obtained for some compounds (**40**, **42**, **45**, and **48** were isolated in 3%, 3%, 4%, and 5% respectively) may relate to electronic and/or steric properties effecting the Suzuki coupling efficiency.

The synthesis of the bicyclic compounds commenced with the acylation of isoindoline (**52**, **54**) and tetrahydroisoquinoline (**53**, **55**–**56**) yielding compounds **57**–**63** (Scheme 2). In addition, isoquinoline **55** was mesylated to form compounds **64**. Bicyclic compounds **68**–**69** (Scheme 3) were generated by converting bromophenylacetic acid (**65**) into secondary amides **66**–**67** using thionyl chloride and methylamine or ethylamine. These were cyclized to the corresponding dihydroisoquinolinones **68**–**69** via a Pictet-Spengler condensation/cyclization with paraformaldehyde, using Eaton's reagent (7.7 wt-% P_2O_5 in $MeSO_3H$) to replace the polyphosphoric acid traditionally used for this cyclization.[38,39] The reaction was initiated with Eaton's reagent activating the aldehyde, followed by the *N*-alkylated amide attacking the activated carbonyl carbon. Dehydration led to alkylideneacetamide formation and after an intramolecular electrophilic aromatic substitution, the dihydroisoquinolinones **68**–**69** were formed in 99% and 94% yield, respectively. Some of the bicyclic amide **69** obtained was dimethylated to yield compound **70**. At this point the generated bicycles (**57**–**64**, **68**–

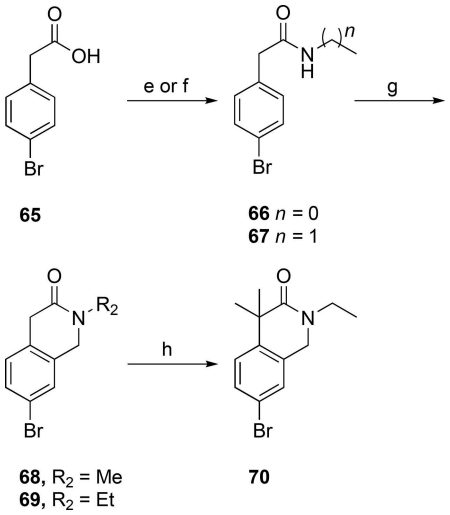

Scheme 3. Synthesis for compounds **68**–**70**. e) 1. Thionyl chloride, DMF, toluene; 2. methylamine, H_2O (to **66**); f) 1. thionyl chloride, DMF, toluene; 2. ethylamine, H_2O (to **67**); g) paraformaldehyde, Eaton's reagent; h) NaH, MeI, DME.

70) were coupled with MIDA boronate **3** under Suzuki conditions in sealed vials using conventional heating, to give compounds **71**–**75**, **77**–**82** (Scheme 4). Isoindoline **54** was also coupled with MIDA boronate **3**, generating compound **76**. Subsequent deprotection and reaction with butyl or ethyl chloroformate produced the sulfonyl butyl carbamate products **83**–**86** and ethyl carbamate products **87**–**96** in moderate to good overall yield (15%–82%), with the exception of compound **94** and **96** that were isolated in 7% and 5% yield, respectively.

2.2. In Vitro Pharmacology

Selectivity for AT_2R over AT_1R was retained for all compounds in series 1, listed in Table 1. Introducing a fluoro substituent in ortho (**40**) or meta (**41**) position relative to the methylene imidazole group resulted in no change in affinity as compared to **C38**. Interestingly, compound **42** with a fluoro atom in the para position to the methylene imidazole exhibited a slight (3-fold) reduction of affinity. This may relate to the altered electronic properties of the molecule or possibly a steric interaction. Replacing the fluoro substituent with methyl in the ortho position to the methylene imidazole was well tolerated (**43**). Adding a methyl to the meta or para position relative to the imidazole (**44** and **45**) did, however, result in a similar reduced affinity as was seen for compound **42**, which further indicates a possible steric interaction. A bromide (**46**) or the larger trifluoromethoxy group (**47**) in the ortho position generated compounds with similar affinity as **C38**. Interestingly, a methoxy group (**48**) in the same position significantly decreased affinity. This may relate to the slightly lower lipophilicity of the methoxy as compared to the trifluoromethoxy moiety, or possibly the electron-donating properties of the substituent. Replacing the phenyl ring for pyridine and placing the nitrogen of the pyridine in the ortho position relative to the methylene imidazole moiety (**49**) furnished a slightly reduced affinity while the equivalent meta and para pyridine analogues (**50**, **51**) exhibit similar affinity for AT_2R as **C38**.

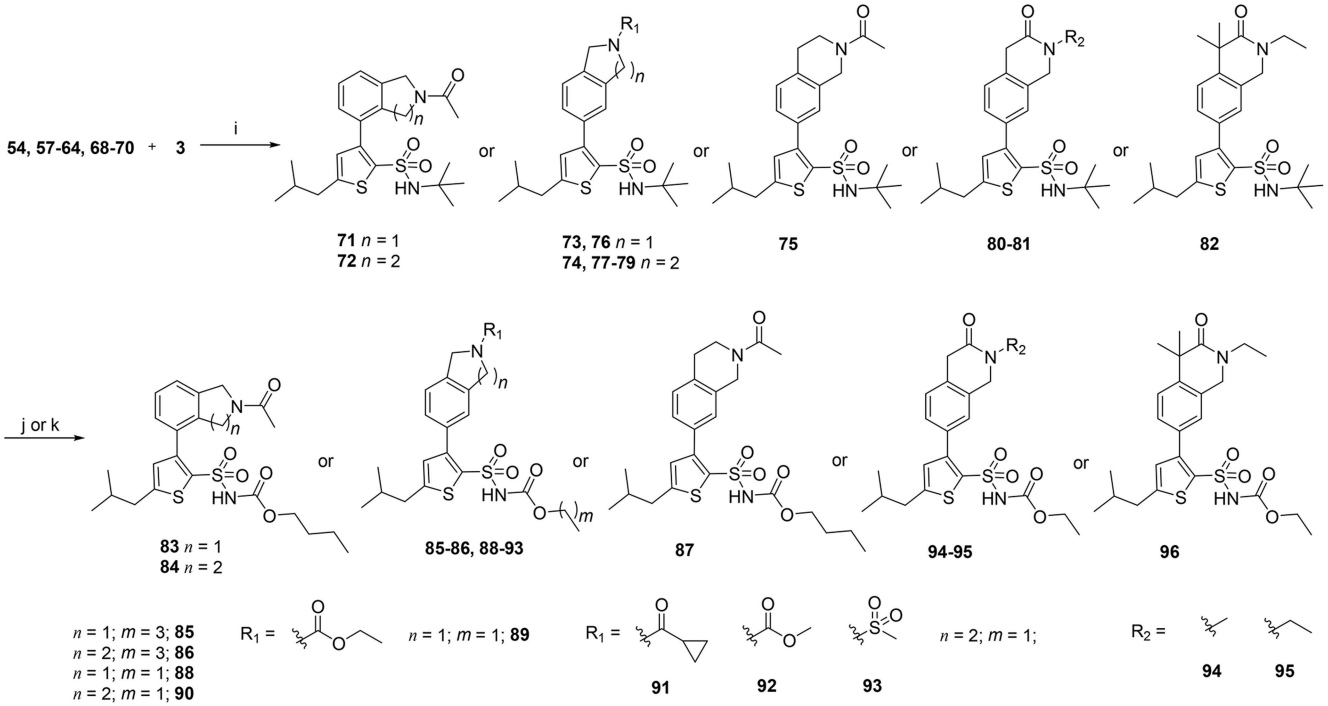

Scheme 4. Synthesis of AT_2R ligands **83**–**96**. i) $PdCl_2$(dppf), K_2CO_3, DME, H_2O; j) 1. TFA; 2. butyl chloroformate, TEA, DCM (to **83**–**87**); k) 1. TFA; 2. ethyl chloroformate, DMAP, DIPEA, DCM (to **88**–**96**).

Table 1. Analogues of **C38** with substituents on the central phenyl ring, synthesized via Scheme 1.

R =

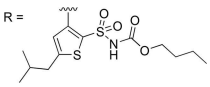

Cmpd	Structure	K_i hAT$_2$R [nM][a]	[%] Inhibition of hAT$_1$R at 10 μM[b]
C38	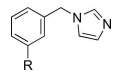	270 (19[c]) IC_{50} = 694 nM[d]	7 IC_{50} > 10 000 nM[e]
40	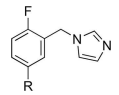	300 IC_{50} = 217 nM[d]	8 IC_{50} > 10 000 nM[e]
41	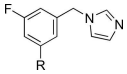	120	13
42	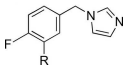	800	16
43	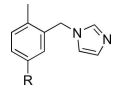	230	14
44	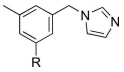	810	26
45	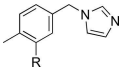	800	12
46	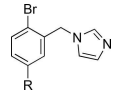	120	18
47	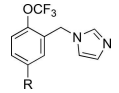	280	1.8
48	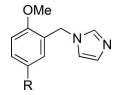	1300	23
49	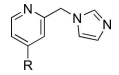	660	19
50	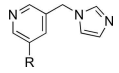	230	22
51	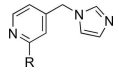	310	9.7

[a] Radioligand displacement from hAT$_2$R in membranes from HEK-293 cells overexpressing hAT$_2$R (assay 1). N = 6 for **C38** and **40**, N = 2 for all other. [b] Inhibition of radioligand binding from hAT$_1$R expressed in HEK-293 cells (assay 1). [c] Radioligand displacement from AT$_2$R in pig uterus membrane.[29] [d] Radioligand displacement from hAT$_2$R expressed in HEK-293 cells (assay 2). [e] Radioligand displacement from hAT$_1$R expressed in HEK-293 cells, ligands were not active on hAT$_1$R at the concentrations tested (assay 2). N = 9.

As we have reported on previously, affinity to human AT$_2$R expressed in HEK-293 cells for **C38** is reduced as compared to affinity for AT$_2$R in pig uterus membrane (270 nM vs 19 nM).[29,35] When evaluating affinity of the previously published, and very promising, amides **C93**, **C97**, and **C102** (Table 2) for human AT$_2$R in HEK-293 cells we note a slight decrease in affinity for compound **C93** (110 nM in human AT$_2$R vs 29 nM in pig AT$_2$R). For compound **C97** the affinity did not change (110 nM in human AT$_2$R vs 83 nM in pig AT$_2$R), but notably for compound **C102** the affinity dropped almost 200-fold (420 nM in human AT$_2$R vs 2.2 nM in pig AT$_2$R). The affinity for human AT$_2$R in HEK-293 cells for the three tested amides were all in the same range as **C38** in the same assay. Similar to the compounds in series 1, the bicyclic derivatives in series 2 (Table 2) also displayed a high selectivity for AT$_2$R. Isoindoline **83** showed a significant reduction in affinity compared to **C93** (> 1500 nM vs 110 nM), suggesting a highly unfavorable orientation of the amide group. The isoquinoline **84**, with similar amide orientation, also displayed reduced affinity. A more favorable amide orientation was obtained in isoindoline **85** and tetrahydroisoquinolines **86** and **87**. Compound **85** and **87** displayed similar affinity as **C38**, while a 5-fold improvement of affinity was seen for compound **86** compared to **C38** (and a 2-fold improvement compared to amides **C93** and **C97**). Having identified the more favorable orientation of the amide, we explored compounds with a shorter and less lipophilic sulfonamide carbamate chain, as well as a few other moieties binding to the amide nitrogen. Interestingly the sulfonyl ethyl carbamate (**88**) resulted in a slightly decreased affinity as compared to the sulfonyl butyl carbamate (**85**).

The affinity was further decreased when introducing a bicyclic *N*-ethyl carbamate in combination with the sulfonamide ethyl carbamate (**89**), displaying a 20-fold drop in affinity as compared to compound **86**. Comparing compound **90** and compound **86**, a slight decrease in affinity could also be detected with the shorter carbamate chain (120 nM vs 56 nM). This indicates the length of the sulfonyl carbamate chain may be more significant in the bicyclic scaffold than in the **C38**-scaffold, where our previous studies showed a large tolerability in this moiety.[35] The cyclopropane carboxamide **91** had a similar affinity as the amides **C93**/**C97** and the bicyclic amide **90**. Interestingly, the bicyclic methyl carbamate **92** was well tolerated in the binding cavity, in contrast to the ethyl carbamate **89** where an almost 5-fold decrease in affinity was observed. The amide bioisosteric mesyl group was introduced in compound **93**, which rendered a reduced affinity to AT$_2$R. Lastly, we had synthesized a three compounds where the carbonyl of the amide function was incorporated as a lactam, locking the amide functionality in a different conformation compared to the previously synthesized bicycles, resulting in the lactam derivatives **94**–**96**. These three compounds all demonstrated a significantly reduced affinity to AT$_2$R.

To ensure quality we assessed three of the compounds and the AT$_2$R agonist **C21** in an orthogonal second assay using whole cells, performed in a different laboratory. The IC_{50} values at both hAT$_2$R and hAT$_1$R were examined for compounds **C38**, **40**, and **86**. The AT$_2$R agonist **C21** exhibited an IC_{50} of 1.47 nM at hAT$_2$R in the orthogonal assay, correlating well with data obtained from the standard assay (K_i = 1.10 nM). Comparing **C38** and **40**, the IC_{50} at hAT$_2$R was improved 3-fold by introducing the para-fluoro, resulting in an estimated 46-fold selectivity for hAT$_2$R over hAT$_1$R (cf. 14-fold hAT$_1$R/hAT$_2$R selectivity for **C38**). It is notable that **C38** and **86** exhibited similar IC_{50} values in the orthogonal assay (**C38**; IC_{50} = 694 nM and **86**; IC_{50} = 818 nM, respectively) although the affinities

Table 2. Bicyclic amides with *N*-ethoxycarbonyl or *N*-butoxycarbonyl sulfonamide moieties synthesized according to Scheme 2–4.

Cmpd	Structure R = 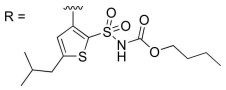	K_i hAT_2R [nM][a]	%-Inhibition of hAT_1R at 10 μM[b]	Cmpd	Structure R = 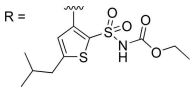	K_i hAT_2R [nM][a]	%-Inhibition of hAT_1R at 10 μM[b]
C93	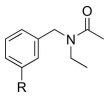	110 (29[c])	22%	**88**	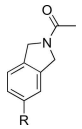	870	7.7%
C97	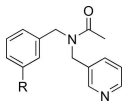	110 (83[c])	23%	**89**	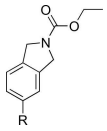	1300	26%
C102	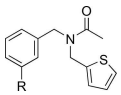	420 (2.2[c])	30%	**90**	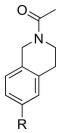	120	NDI[g]
83	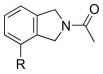	>1500[d]	15%	**91**	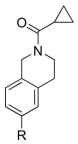	120	28%
84	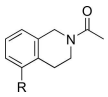	700	22%	**92**	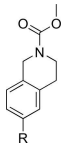	290	15%
85	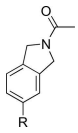	360	7.5%	**93**	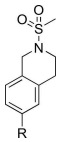	760	19%
86	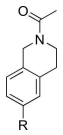	56 IC_{50} = 818 nM[e]	34% IC_{50} > 10 000 nM[f]	**94**	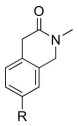	1300	1.5%
87	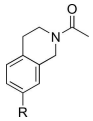	270	45%	**95**	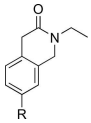	850	11%
–	–	–	–	**96**	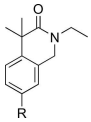	1100	15%

[a] Radioligand displacement from hAT_2R in membranes from HEK-293 cells overexpressing hAT_2R (assay 1). N = 2. [b] Inhibition of radioligand binding from hAT_1R expressed in HEK-293 cells (assay 1). [c] Radioligand displacement from AT_2R in pig uterus membrane.[29] [d] K_i estimated to more than 1500 nM, IC_{50} was determined to be > 3 000 nM. [e] Radioligand displacement from hAT_2R expressed in HEK-293 cells (assay 2). [f] Radioligand displacement from hAT_1R expressed in HEK-293 cells, ligands were not active on hAT_1R at the concentrations tested (assay 2). N = 9 [g] NDI = no detectable inhibition.

differed considerably in the standard assay applied herein (**C38**; K_i = 270 nM and **86**; K_i = 56 nM, respectively).

2.3. Molecular Modelling

Using the published crystal structure of AT_2R[34], a comprehensive docking exploration with GLIDE revealed a common binding pose for the compounds in the first series (Table 1), which in each case was refined by MD equilibration.

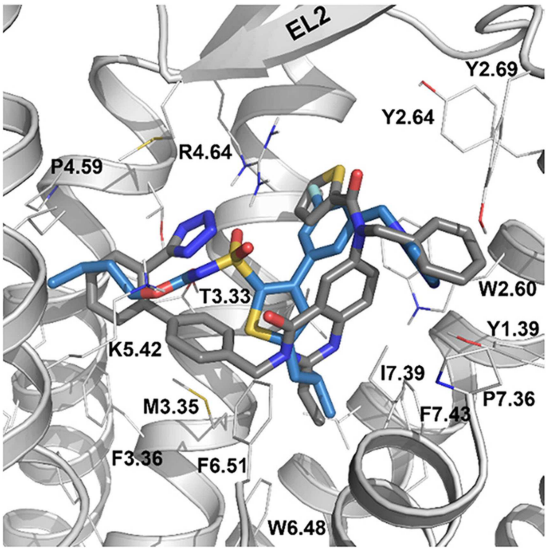

Figure 2. Compound **41** (blue) biding to the AT_2 receptor (gray), overlaid with the co-crystalized ligand L-161,638 (PDB 5UNG, gray sticks).

Figure 2 depicts the binding mode for the most potent compound (**41**) in series 1, overlaid with the co-crystalized AT_2R antagonist L-161,638. The sulfonyl carbamate is anchored via salt-bridge interactions with $R182^{4.64}$ and $K215^{5.42}$ and a hydrogen bond of the carbonyl with $T125^{3.33}$ (the Ballesteros-Weinstein generic amino acid numbering scheme is indicated as superscript[40]). The phenyl ring is surrounded by $W100^{2.60}$ and $L124^{3.32}$, allowing the imidazole substituent to be accommodated within a hydrophobic cluster composed by residues $Y51^{1.39}$, $Y103^{2.64}$, $Y104^{2.65}$, $Y108^{2.69}$, $P301^{7.36}$ and $I304^{7.39}$. The isobutyl group is placed in a deeper region of the transmembrane cavity, defined by residues $L124^{3.32}$, $M127^{3.35}$, $W269^{6.48}$, $F272^{6.51}$, and $F308^{7.43}$. Finally, the ethyl substituent on the sulfonyl carbamate is located in the cavity between transmembrane helices TM3-TM5 defined by the residues $Pro177^{4.59}$, $Met214^{5.41}$, $Lys215^{5.42}$, and $F129^{3.37}$.

The binding mode proposed explains to a big extent the SAR for the compounds in the first series (Figure 3), which are structurally related to the prototype antagonist **C38**. The

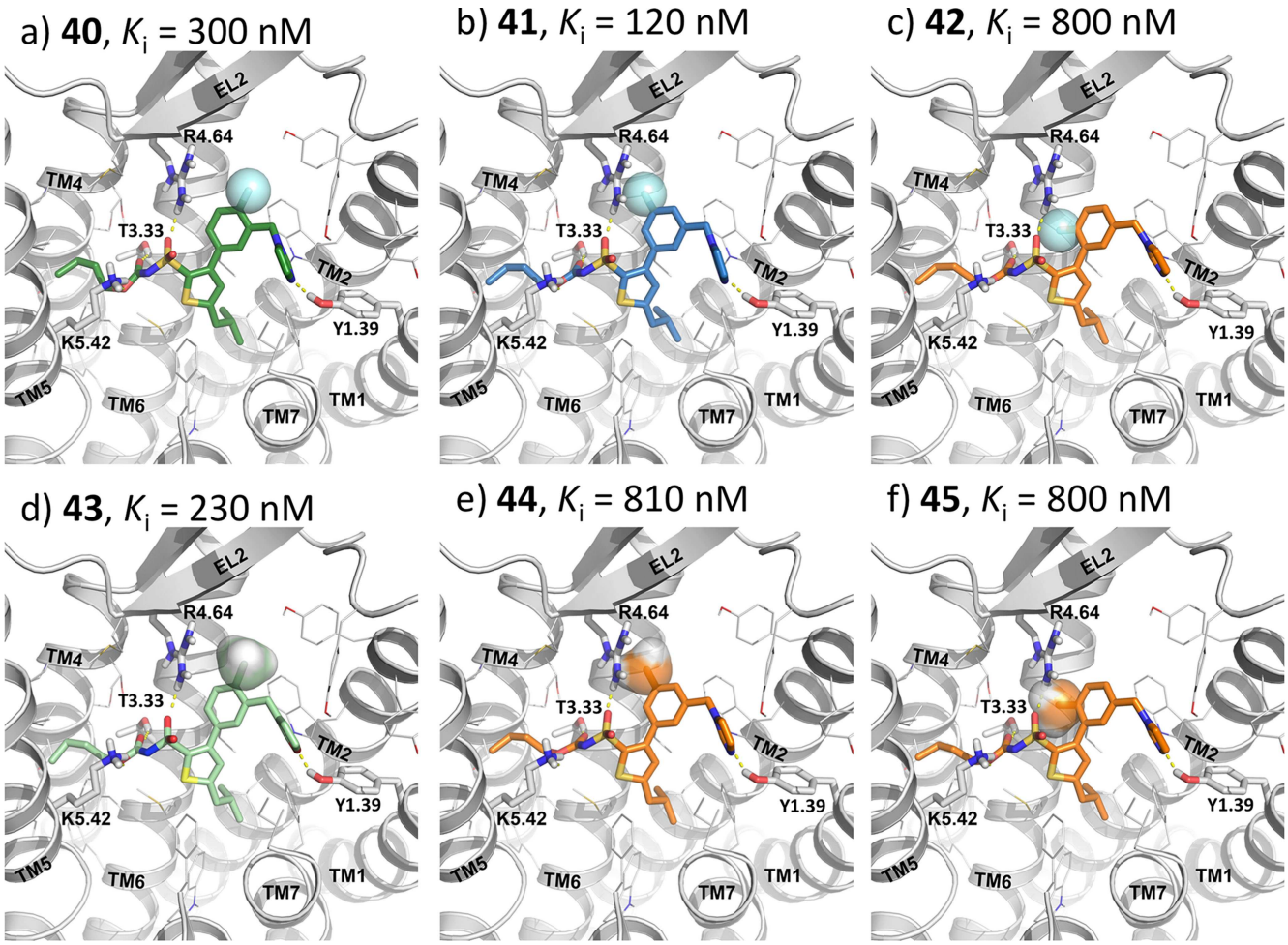

Figure 3. The docked ligands (**40**–**45**) in the most common pose on the modeled conformation of the AT_2R. The ligands are color coded based on the binding affinities, blue – high, green – moderate, and orange – low binding affinity. The N-terminal, EL3 and parts of TM6-TM7 of the AT_2R are not shown for better clarity.

experimental affinities (Table 1) show that introduction of a fluoro substituent in ortho position (**40**) relative to the methylene imidazole substituent is well tolerated, as is introducing a methyl group in the ortho position to the imidazole (**43**). This is consistent with the modelling of these substituents located in a cavity pointing towards the extracellular side (Figure 3a and Figure 3d). A meta-fluoro substitution (**41**) slightly improves the affinity, probably due to favorable electrostatic interactions with Arg182$^{4.64}$ (Figure 3b).

Interestingly, compound **42** with a fluoro atom in the para position to the imidazole exhibited a slight (3-fold) reduction of affinity. The interaction with Arg182$^{4.64}$ cannot occur for compound **42** (Figure 3c), due to an electrostatic repulsion to the carbonyl of the sulfonyl carbamate. Adding a methyl to the meta or para position relative to the methylene imidazole (**44** and **45**) also result in a similar reduced affinity as was seen for compound **42**, which correlates with a sub-optimal fitting in the site between Arg182$^{4.64}$ and Trp100$^{2.61}$ as indicated in Figure 3e and 3f.

The pharmacological profile of the compounds in the second series has not been assessed due to lack of reliable functional biological models. The related amides reported by our group in 2012 displayed both agonistic and antagonist properties indicating a complex pharmacological relationship for ligands deviating from the imidazole head group[29]. Hence, tentative binding modes of the ligands in the second series were not studied in the antagonist binding model presented herein.

Table 3. Compounds evaluated for stability in mouse and human liver microsome assay. The kinetic solubility was also determined for a selection of compounds.

Cmpd	HLM $t^1/_2$ [min][a]	MLM $t^1/_2$ [min][a]	Kinetic solubility [μM][b]
C38	12	70	90
C93	15	5.8	72
40	12	88	81
41	7.3	41	52
42	7.8	48	ND[c]
43	11	39	37
44	7.0	35	24
45	5.2	11	46
46	5.1	99	21
47	10	103	52
48	5.3	31	32
49	7.6	6.5	50
50	17	18	58
51	7.6	13	44
83	15	6.9	ND[c]
84	6.4	3.8	ND[c]
85	2.4	1.8	30
86	8.7	2.9	45
87	5.4	2.2	31
88	7.8	21	35
89	2.3	2.1	58
90	32	14	76
91	13	7.4	47
92	13	12	60
93	22	4.6	ND[c]
94	7.8	23	61
96	25	3.9	78

[a] The metabolic stability was determined in 0.5 mg/mL human or mouse liver microsomes for compounds at a concentration of 1 μM in potassium phosphate buffer. [b] The kinetic solubility was determined at a final compound concentration of 100 μM in potassium phosphate buffer with 1% DMSO. [c] ND = Not determined.

2.4. Stability in Liver Microsomes and Kinetic Solubility

Table 3 lists compounds that were evaluated for metabolic stability in human and mouse liver microsomes (HLM/MLM). For a selection of compounds the kinetic solubility was also determined. The previously reported AT_2R ligands **C38** and **C93** were also, for comparison, evaluated in the same assays.[29] The parent compound **C38** exhibited a moderate stability in both human (12 min) and mouse (70 min) liver microsomes. All analogues related to the imidazole derivative **C38** displayed a similar trend, with the compounds being more prone to undergo metabolism in human microsomes. Introduction of a fluoro atom onto phenyl rings is a well-known strategy in medicinal chemistry to block phase I metabolism (oxidation), a potential problem suggested for **C38**.[41,42] Adding a fluoro atom encouragingly displayed a retained affinity for AT_2R (**40**, **41**, Table 1). Unfortunately, the metabolic stability in human liver microsomes was not improved for any of the fluorinated compounds (**40**, **41**, and **42**). In mouse liver microsomes the metabolic stability was only retained for the ortho fluorinated compound (**40**) (Table 3). This implies that the phenyl ring is likely not the main site for oxidative metabolism of **C38** in human liver microsomes. The solubility of fluoro-analogue **40** was similar to **C38** but was interestingly reduced for compound **41**. Methylation of the phenyl ring produced slightly more lipophilic ligands (**43-46**), for which the affinity could only be retained for compound **43**. The metabolic stability was unsurprisingly reduced for these compounds, as they are likely better substrates for benzylic oxidation than **C38**. Methyl analogues **43**–**45** also displayed reduced solubility, likely related to the added lipophilicity.

The bromo and trifluoromethoxy derivatives **46** and **47** displayed a retained stability profile in both mouse and human liver microsomes (Table 3). For methoxy compound **48** the metabolic stability was reduced. Introducing the bromo, trifluoromethoxy and methoxy resulted in reduced solubility compared to **C38**. Attempts to improve solubility of **C38** by exchanging the phenyl ring for a pyridine gave unsatisfying results. Although exhibiting similar affinity as **C38** the solubility was reduced for all three pyridine compounds **49**–**51**. Moreover, the metabolic stability of the pyridines in mouse liver microsome assay was also reduced as compared to **C38**.

The solubility and stability in human liver microsomes of the amide **C93** were similar to **C38**. Notably, in mouse liver microsomes the metabolic stability of **C93** was significantly reduced as compared to **C38**. All of the bicyclic amides in the series demonstrated very low stability in mouse microsomes, with two exceptions (compound **88** and **94**). For example, the bicyclic amides **85**, **86**, **87**, and **89** rapidly decompose and are similarly unstable in human microsomes. The solubility was also reduced compared to the non-cyclized amide **C93**. Neither the bicyclic acetyl amide **83** nor **84**, regioisomers of **85** and **86**, respectively, demonstrated any improved metabolic profile.

Comparing the butyloxycarbonyl sulfonamide **85**, one of the most metabolically unstable compounds in this report, with the corresponding ethoxycarbonyl compound **88** reveals only a slightly improved stability in mouse liver microsomes for the latter. A larger increase was expected in accordance with previously reported data.[35] A larger impact on stability in human microsomes with a shortened carbamate alkyl chain can be noted when comparing **86** and with **90**. The very low stability of the bicyclic amide **86** is unfortunate as compound **86** exhibits the highest affinity of all compounds assessed. Exchanging the acetyl of compound **90** gave the equipotent acetyl propyl **91** and carbamate **92**, neither of which showed any improved solubility or metabolic stability. The bioisosteric sulfonamide **93** exhibit a metabolic stability of more than 20 min in human microsomes. The same was seen for compound **96**, however both **93** and **96** are poor AT_2R binders. The solubility was only comparable to **C93** for compounds **90** and **96**.

3. Conclusion

In summary, two series of new AT_2R ligands were synthesized and evaluated. In the first series, small structural changes were introduced to the central phenyl ring of the known AT_2R antagonist **C38**. These were well-tolerated with half of the compounds synthesized exhibiting similar or slightly improved affinity to AT_2R compared to **C38**. A common binding pose was identified for the compounds in the first series, a pose that could ascribe the reduced affinity for 3 out of 4 low-affinity compounds to a sub-optimal fit between Arg182 on helix TM4 and Trp100 on helix TM2. The highest affinity in the first series was displayed by the meta fluoro derivative **41** and the ortho bromo substituted derivative **46**, of which only the latter displayed retained metabolic stability in mouse liver microsomes. In the second series where the imidazole heterocycle of **C38** was replaced by bicyclic amides, the most favorable amide orientation was identified and explored. Compound **86** displayed the highest affinity to AT_2R of all compounds assessed ($K_i = 56$ nM at AT_2R). Unfortunately, all compounds in the second series exhibited a low metabolic stability both in human and mouse liver microsomes. The stability could be slightly improved by reducing the sulfonyl carbamate chain length (cf. compound **85** vs **88**, and compound **86** vs **90**).

Experimental Section

General Chemistry

All chemicals and solvents were purchased from Sigma Aldrich, Fisher Scientific, FluoroChem, and Enamine, and were used without further purification. Microwave heating was performed in a Biotage Initiator + single-mode microwave reactor. Automated flash column chromatography was performed on Biotage Isolera or Grace Reveleris instruments using commercial silica cartridges. Manual flash chromatography was performed on silica gel 60. Preparative reverse-phase HPLC was performed using a C18 column with UV detection. Analytical HPLC/ESI-MS was performed using electrospray ionization (ESI) and a C18 column. High resolution molecular masses (HRMS) were determined on a mass spectrometer equipped with an ESI source and 7-T hybrid linear ion trap (LTQ). NMR spectra were recorded at 400 MHz for ^1H and 101 MHz for ^{13}C.

Synthesis

Butyl ((3-(2-acetyl-1,2,3,4-tetrahydroisoquinolin-6-yl)-5-isobutylthiophen-2-yl)sulfonyl)carbamate (86)

A 20 mL vial containing $ZnCl_2$ (1.7 eq.) was dried in a vacuum oven at 120 °C overnight. The vial was capped and evacuated twice with vacuum/N_2(g). After cooling to room temperature the $ZnCl_2$ was dissolved in dry THF (5 mL). Isobutylmagnesium chloride (2 M in THF; 1.5 eq.) was added dropwise. After 10 min of stirring, a solution of 5-bromo-*N*-(*tert*-butyl)thiophene-2-sulfonamide (**1**, 7.3 mmol, 1.0 eq.) and Pd(*t*-$Bu_3P)_2$ (0.015 eq.) in dry toluene (5 mL) was added. The mixture was microwave heated at 130 °C for 15 min after which it was partitioned between DCM and sat. aq. NH_4Cl (3:2). The aqueous layer was extracted with DCM and the combined organic layers were washed with brine, dried with $MgSO_4$ and concentrated under reduced pressure. The remaining residue was purified using silica gel flash chromatography (isohexanes with 10% (v/v) EtOAc). *N*-(*tert*-Butyl)-5-isobutylthiophene-2-sulfonamide (**2**) was isolated in 51% yield.[35,43]

N-(*tert*-Butyl)-5-isobutylthiophene-2-sulfonamide (**2**, 8.2 mmol, 1.0 eq.) was dissolved in dry THF (70 mL) and transferred to a dry three-necked round bottom flask. The flask was cooled to −78 °C and evacuated thrice with vacuum/N_2(g). To this was added *n*-butyllithium (2.5 M in hexane; 4.5 eq.) dropwise after which the mixture was stirred for 1 h at −78 °C. The reaction was subsequently stirred at 0 °C for 1 h, after which it was again cooled to −78 °C and triisopropyl borate (2.5 eq.) was added. After 15 min the flask was again stirred at 0 °C for 3 h. The mixture was quenched with 2 M HCl (aq.) and partially evaporated before it was diluted with water and the product was extracted with DCM. The combined organic layers were dried with $MgSO_4$ and the solvent was removed under reduced pressure. The crude residue was dissolved in DMSO (2 mL) and toluene (30 mL), methyliminodiacetic acid (1.3 eq.) was added and the mixture was refluxed for 3 h. The mixture was diluted with EtOAc and washed with 0.1 M HCl (aq.). The organic phase was dried with $MgSO_4$ and the solvent was removed under reduced pressure. The residue obtained was dissolved in minimal amounts of acetone and equal amounts of diethyl ether after which hexane (100 mL) was added using a dropping funnel. The solid formed was filtered off and submitted to the same precipitation procedure once more. *N*-(*tert*-Butyl)-5-isobutyl-3-(6-methyl-4,8-dioxo-1,3,6,2-dioxazaborocan-2-yl)thiophene-2-sulfonamide (**3**) was collected in 76% yield.[35]

6-Bromo-1,2,3,4-tetrahydroisoquinoline (**55**, 0.44 mmol, 1.0 eq.) and K_2CO_3 (2.3 eq.) were dissolved in MeCN (4 mL). Acetic anhydride (1.4 eq.) was added and the mixture was stirred overnight. The solvent was removed under reduced pressure and the product was purified by silica gel column chromatography (DCM with 5% (v/v) MeOH). 1-(6-Bromo-3,4-dihydroisoquinolin-2(1*H*)-yl)ethan-1-one (**60**) was isolated in 97% yield as 2 amide rotamers in 60:40 ratio at room temperature. ^1H NMR (400 MHz, DMSO-d_6, T = 373 K) δ 7.45–7.28 (m, 2H), 7.21–7.09 (m, 1H), 4.57 (s, 2H), 3.65 (t, $J = 6.0$ Hz, 2H), 2.84 (m, 2H), 2.07 (s, 3H). ^{13}C NMR (101 MHz, DMSO-d_6, T = 353 K) δ 168.2, 130.5, 130.2, 130.1, 128.6, 128.0, 118.8, 42.7, 38.9, 28.9, 20.8.

MIDA-boronate (**3**, 0.20 mmol, 1.0 eq.), K_2CO_3 (5.0 eq.), 1-(6-bromo-3,4-dihydroisoquinolin-2(1*H*)-yl)ethan-1-one (**60**) (1.0 eq.), and

$PdCl_2(dppf)$ (0.05 eq.) were dissolved in DME (1 mL) and water (0.2 mL) in a 2–5 mL vial. The vial was flushed with N_2 and the mixture was heated at 120 °C for 1 h. The reaction mixture was diluted with EtOAc and the layers were separated. The organic layer was purified by automated silica flash chromatography (isohexane with 50–100 % (v/v) EtOAc). The fractions containing product were collected and the solvent removed under reduced pressure. The crude 3-(2-acetyl-1,2,3,4-tetrahydroisoquinolin-6-yl)-*N*-(*tert*-butyl)-5-isobutylthiophene-2-sulfonamide (**74**) was stirred in TFA (99.9 %; 65 eq.) at 40 °C overnight. The TFA was removed and the remaining crude material was dissolved in DCM (2 mL). To this was added triethylamine (2.1 eq.) and the mixture was stirred for 10 min at room temperature, after which butyl chloroformate (0.7 eq.) was added and the mixture was stirred at room temperature for 1 h. The reaction mixture was washed with 2 M HCl (aq.) and brine and dried with $MgSO_4$. The solvent was evaporated and the product was purified by preparative RP-HPLC (20-100 % MeCN in water (0.05 % formic acid)). Butyl ((3-(2-acetyl-1,2,3,4-tetrahydroisoquinolin-6-yl)-5-isobutylthiophen-2-yl)sulfonyl)carbamate (**86**) was obtained in 28 % yield over 2 steps as a mixture of 2 amide rotamers in 60:40 ratio. ^{1}H NMR (400 MHz, Chloroform-*d*) δ 7.93 (overlapping; s, 2H), 7.35–7.28 (overlapping; m, 2H), 7.26–7.22 (overlapping; m, 2H), 7.19–7.12 (overlapping; m, 2H), 6.743 (minor; s, 1H), 6.737 (major; s, 1H), 4.74 (major; s, 2H), 4.65 (minor; s, 2H), 4.07 (minor; t, J = 6.6, 2H), 4.06 (major; t, J = 6.6, 2H), 3.81 (minor; t, J = 5.9 Hz, 2H), 3.69 (major; t, J = 5.9 Hz, 3H), 2.93 (major; t, J = 5.9 Hz, 3H), 2.85 (minor; t, J = 6.0 Hz, 2H), 2.70 (d, J = 7.1 Hz, 4H), 2.18 (minor; s, 3H), 2.17 (major; s, 3H), 1.93 (overlapping; m, 2H), 1.52 (overlapping; m, 4H), 1.27 (overlapping; m, 4H), 0.99 (overlapping; d, J = 6.6 Hz, 12H), 0.89 (overlapping; t, J = 7.4 Hz, 6H). ^{13}C NMR (101 MHz, Chloroform-*d*) δ 169.8, 169.7, 151.7, 151.6, 150.4, 146.4, 146.3, 135.2, 134.2, 134.1, 133.2, 132.9, 132.6, 130.9, 129.64, 129.60, 129.5, 129.1, 127.3, 127.2, 126.7, 126.2, 67.0, 66.9, 48.1, 44.1, 44.0, 39.5, 30.7, 30.6, 29.5, 28.6, 22.4, 22.0, 21.7, 18.9, 13.7. MS (ESI): *m/z* calc'd for $C_{24}H_{32}N_2O_5S_2$: 491.1674 $[M-H]^-$; found: 491.1664

Further details on reaction conditions is available for all reactions in the supporting information. ^{1}H NMR spectra were generated for all final compounds. Purity and elemental analyses were performed on all final compounds. ^{13}C spectra were generated for a majority of the final compounds. All available spectral analysis is reported in the supplementary information.

Binding Assays

Assay 1 (K_i Determination)

All synthesized ligands were evaluated in a radioligand assay by displacing [^{125}I][Sar^{1}Ile^8]-angiotensin II from human AT_2R in HEK-293 cells membrane preparations. [Sar^{1}Ile^8]-angiotensin II (Sarile) acts as a nonselective AT_2R agonist.[44] The affinity was determined using a seven-point dose-response curve, each point performed in duplicates. All dose-response curves are available in the Supplementary Information. Each new assay was validated using a selection of known ligands in accordance with Eurofins Cerep standard protocol. The compounds were also evaluated for inhibition of [^{125}I][Sar^{1}Ile^8]-angiotensin II binding to human AT_1R in HEK-293 cell membranes. For AT_1R the percent inhibition was determined at 10 μM, in duplicates, with the endogenous ligand (angiotensin II) used as reference.

Assay 2 (IC_{50} Determination)

The IC_{50} values of **C38**, **40**, **86** and **C21** were assessed in whole cells assay using HEK293 cells expressing AT_1R or AT_2R as described previously[45–47]. Cells were grown to approximately 80 % confluence before being re-plated into 48 well plates at 1×10^5 cells/well and grown for 48 h at 37 °C for a whole cell competition binding assay. [^{125}I]-Sar^{1}Ile^{8}Ang II at 50,000 cpm, incubated for 45 min at 37 °C, in the absence or presence of unlabeled ligands, prepared in binding buffer (DMEM, 0.1 % BSA), were used in the competition assays at concentrations ranging from 1 pM to 10 μM. For each experiment, each ligand concentration was tested in triplicate, and each experiment was repeated at least 3 separate times. Non-specific binding (NSB) was defined in the presence of the unlabeled Ang II (10 μM). The ability of each ligand to inhibit specific binding of [^{125}I]-Sar^{1}Ile^{8}Ang II was measured on a gamma counter with all counts corrected for NSB. Non-linear regression of the data using one-site fit model was performed and IC_{50} values, representing the concentration at which each ligand displaced 50 % of [^{125}I]-Sar$_1$Ile$_8$Ang II binding, were calculated as affinity estimates for each ligand at AT1R and AT2R, using GraphPad Prism 6 (GraphPad Software Inc., San Diego, CA, USA).

Kinetic Solubility

The kinetic solubility was investigated for compounds **40**–**41**, **43**, **46**–**48**, **50**–**51**, **85**–**92**, **94**, **96**. Kinetic solubility was measured at a final compound concentration of 100 μM and 1 % DMSO in 100 mM potassium phosphate buffer (pH 7.4) and incubated at 37 °C for at least 20 h. After incubation, the samples are centrifuged at 3000xg at 37 °C for 30 min to pellet insoluble material and an aliquot of the supernatant was taken for quantification of compound concentration by LC-MS/MS analysis. The LC-MS/MS system was an Acquity UPLC coupled to a triple quadrupole mass spectrometer (Waters), operating in multiple reaction monitoring (MRM) mode with positive or negative electrospray ionization. Mass spectrometric settings were optimized for each compound for one MRM transition. Chromatographic separation was typically done on a C18 Ethylene Bridged Hybrid (BEH) 1.7 μm column using a general gradient of 1 % to 90 % of mobile phase consisting of A, 5 % acetonitrile and 0.1 % formic acid in purified water, and B, 0.1 % formic acid in 100 % acetonitrile, over a total running time of 2 min. In a few cases, separation was done on a HSS T3 2×50 mm 2.1 μm column using a mobile phase consisting of A, 0.05 % heptafluorobutyric acid (HFBA) and 0.05 % propionic acid (PA) in water, and B, 0.05 % HFBA and 0.05 % PA in acetonitrile, with a total running time of 2 min. In both cases, the flow rate was set to 0.5 mL/min and 5 μL of the sample was injected.

Stability in Liver Microsomes

Human and mouse liver microsomes were used to assess the metabolic stability for all compounds (**95** excluded). Metabolic stability was determined in 0.5 mg/mL human or mouse liver microsomes at a compound concentration of 1 μM in 100 mM potassium phosphate buffer (pH 7.4) in a total incubation volume of 500 μL. The reaction was initiated by addition of 1 mM NADPH. At various incubation times, i.e. at 0, 5, 10, 20, 40 and 60 min, a sample was withdrawn from the incubation and the reaction was terminated by addition of ice-cold acetonitrile containing Warfarin as internal standard. The amount of parent compound remaining was analyzed by LC-MS/MS as described above (Kinetic Solubility). *In vitro* half-life ($t_{1/2}$) and in vitro intrinsic clearance (Cl_{int}) were calculated using previously published models.[48,49] Extraction ratio (E), i.e. the ratio of the hepatic clearance of a drug to the hepatic blood flow, can be generally classified as high (>0.7), intermediate (0.3–0.7) or low (<0.3), according to the fraction of drug removed during one pass through the liver. For human and mouse liver

microsomes, E of 0.3 and 0.7 would correspond to a $t_{1/2}$ of 126 min and 23 min, and 193 min and 35 min, respectively.

Molecular Modelling of the AT_2 Receptor

The crystal structure of the human AT_2R was retrieved from the Protein Data Bank (PDB code 5UNG with antagonist L-161,638)[31,34] and was subject to preparation and minor modifications with the Schrödinger suite (Schrödinger Release 2017–3, Schrödinger, LSS, New York, NY, 2017), including (i) deletion of the engineered B_{562}RIL protein (fused to the truncated N-terminus); (ii) addition of protons, assessment of the rotamers for Asn/Gln/His residues, and protonated state for titratable residues, resulting in all Asp, Gln, Lys, and Arg residues assigned to their default charged state and all His modelled as neutral with the proton on Nδ; (iii) addition of missing side chains, modelling the most probable conformer based on additional crystal structures of AT_2 and the related AT_1 receptor.

Ligand Docking

Ligands from Tables 1 were built and optimized their 3D conformation using the Maestro graphical interface and the LigPrep utility from the Schrödinger suite (Schrödinger Release 2017–3: Maestro, Schrödinger, LSS, New York, NY, 2017; Schrödinger Release 2017-3: LigPrep, Schrödinger, LSS, New York, NY, 2017). This method also allowed determination of their most probable protonation state at physiological pH, with a net negative change localized on the sulfonylcarbamate group in all cases. Docking was performed with Glide SP using default settings (Schrödinger Release 2017–3: Glide, Schrödinger, LSS, New York, NY, 2017).[50–52] The docking grid was placed taking as reference the coordinates of the co-crystallized ligand L-161,638, and expanding the cubic grid box to 30 Å on each dimensions. The selection of poses was done on the basis of a double criteria, combining the highest possible scoring while looking for the consensus among all ligands in the series.

Membrane Insertion and Molecular Dynamics Equilibration

Each ligand-receptor complex obtained in the previous stage was subject to an MD equilibration following the PyMedDyn protocol, as implemented in a GPCR-ModSim web server.[53,54] Briefly, the receptor-ligand complex was inserted in a pre-equilibrated membrane consisting of 1-palmitoyl-2-oleoyl phosphatidylcholine (POPC) lipids, with the transmembrane (TM) bundle aligned to its vertical axis. The simulation box was created with a hexagonal-prism geometry, which was soaked with bulk water and energy-minimized using the OPLS-AA force field for proteins and ligands, combined with the Berger parameters for the lipids.[53,55–57] It follows a molecular dynamics equilibration using periodic boundary conditions (PBC) and the NPT ensemble with the GROMACS simulation package.[55]

The first phase consists of 2.5 ns with a gradual release of harmonic restraints on protein (and ligand) heavy atoms. The second phase consists of free MD for another 2.5 ns, except for weak distance restraints between 24 pairs of interacting residues corresponding to conserved positions within the TM bundle of class-A GPCRs with a structural role.[54,58] The final snapshot was energy minimized and retained for analysis and figures.

Acknowledgements

We thank the SciLifeLab Drug Discovery and Development Platform for support with compound synthesis and ADME evaluations, the Swedish National Infrastructure for Computing (SNIC) for synthetic and computational resources, the Kjell and Märta Beijer Foundation and the Swedish Research Council for financial support.

Conflict of Interest

The authors declare no conflict of interest.

Keywords: AT_2 receptor · angiotensin II · medicinal chemistry · molecular docking · prototype antagonist

[1] M. Hallberg, *Med. Res. Rev.* **2015**, *35*, 464–519.
[2] S. Whitebread, M. Mele, B. Kamber, M. de Gasparo, *Biochem. Biophys. Res. Commun.* **1989**, *163*, 284–291.
[3] A. T. Chiu, W. F. Herblin, D. E. McCall, R. J. Ardecky, D. J. Carini, J. V. Duncia, L. J. Pease, P. C. Wong, R. R. Wexler, A. L. Johnson, *Biochem. Biophys. Res. Commun.* **1989**, *165*, 196–203.
[4] S. H. Padia, R. M. Carey, *Pflügers Arch. – Eur. J. Physiol.* **2013**, *465*, 99–110.
[5] S. Foulquier, U. M. Steckelings, T. Unger, *Nature* **2013**, *493*, S9.
[6] T. Unger, U. M. Steckelings, R. A. S. dos Santos, *The Protective Arm of the Renin Angiotensin System*, Elsevier, **2015**.
[7] E. F. Grady, L. A. Sechi, C. A. Griffin, M. Schambelan, J. E. Kalinyak, *J. Clin. Invest.* **1991**, *88*, 921–933.
[8] N. R. Bastien, G. M. Ciuffo, J. M. Saavedra, C. Lambert, *Regul. Pept.* **1996**, *63*, 9–16.
[9] M. De Gasparo, K. J. Catt, T. Inagami, J. W. Wright, T. Unger, *Pharmacol. Rev.* **2000**, *52*, 415–472.
[10] "AGT2R," can be found under https://www.proteinatlas.org/ENSG00000180772-AGTR2/tissue, **2018**.
[11] U. M. Steckelings, F. Rompe, E. Kaschina, P. Namsolleck, A. Grzesiak, H. Funke-Kaiser, M. Bader, T. Unger, *J. Renin. Angiotensin. Aldosterone. Syst.* **2010**, *11*, 67–73.
[12] C. Sumners, A. D. De Kloet, E. G. Krause, T. Unger, U. M. Steckelings, *Curr. Opin. Pharmacol.* **2015**, *21*, 115–121.
[13] M. Nakajima, H. G. Hutchinson, M. Fujinaga, W. Hayashida, R. Morishita, L. Zhang, M. Horiuchi, R. E. Pratf, V. J. Dzau, R. W. Berliner, *Proc. Mont. Acad. Sci.* **1995**, *92*, 10663–10667.
[14] S. Gallinat, M. Yu, A. Dorst, T. Unger, T. Herdegen, *Mol. Brain Res.* **1998**, *57*, 111–122.
[15] W. Altarche-Xifro, C. Curato, E. Kaschina, A. Grzesiak, S. Slavic, J. Dong, K. Kappert, M. Steckelings, H. Imboden, T. Unger, *Stem Cells* **2009**, *27*, 2488–2497.
[16] S. Busche, S. Gallinat, R.-M. Bohle, A. Reinecke, J. Rg Seebeck, F. Franke, L. Fink, M. Zhu, C. Sumners, T. Unger, *Am. J. Pathol.* **2000**, *157*, 605–611.
[17] Y. Nio, H. Matsubara, S. Murasawa, M. Kanasaki, M. Inada, *Clin. Invest.* **1995**, *95*, 46–54.
[18] J. Li, J. Culman, H. Hörtnagl, Y. Zhao, N. Gerova, M. Timm, A. Blume, M. Zimmermann, K. Seidel, U. Dirnagl, *FASEB J.* **2005**, *16*, 617–619.
[19] M. T. Smith, B. D. Wyse, S. R. Edwards, *Pain Med.* **2013**, *14*, 692–705.
[20] A. S. C. Rice, R. H. Dworkin, T. D. McCarthy, P. Anand, C. Bountra, P. I. McCloud, J. Hill, G. Cutter, G. Kitson, N. Desem, *Lancet* **2014**, *383*, 1637–1647.
[21] Y. Wan, C. Wallinder, B. Plouffe, H. Beaudry, A. K. Mahalingam, X. Wu, B. Johansson, M. Holm, M. Botros, A. Karlén, *J. Med. Chem.* **2004**, *47*, 5995–6008.
[22] M. Larhed, M. Hallberg, A. Hallberg, *Med. Chem. Rev.* **2016**, *51*, 69–82.
[23] M. Hallberg, C. Sumners, U. M. Steckelings, A. Hallberg, *Med. Res. Rev.* **2018**, *38*, 602–624.
[24] X. Wu, Y. Wan, a K. Mahalingam, a M. S. Murugaiah, B. Plouffe, M. Botros, A. Karlén, M. Hallberg, N. Gallo-Payet, M. Alterman, *J. Med. Chem.* **2006**, *49*, 7160–8.

[25] A. M. S. Murugaiah, C. Wallinder, A. K. Mahalingam, X. Wu, Y. Wan, B. Plouffe, M. Botros, A. Karlén, M. Hallberg, N. Gallo-Payet, *Bioorg. Med. Chem.* **2007**, *15*, 7166–83.
[26] J. Georgsson, C. Sköld, M. Botros, G. Lindeberg, F. Nyberg, A. Karlén, A. Hallberg, M. Larhed, *J. Med. Chem.* **2007**, *50*, 1711–1715.
[27] C. Wallinder, M. Botros, U. Rosenström, M.-O. Guimond, H. Beaudry, F. Nyberg, N. Gallo-Payet, A. Hallberg, M. Alterman, *Bioorg. Med. Chem.* **2008**, *16*, 6841–9.
[28] A. K. Mahalingam, Y. Wan, A. M. S. Murugaiah, C. Wallinder, X. Wu, B. Plouffe, M. Botros, F. Nyberg, A. Hallberg, N. Gallo-Payet, *Bioorg. Med. Chem.* **2010**, *18*, 4570–90.
[29] A. M. S. Murugaiah, X. Wu, C. Wallinder, A. K. Mahalingam, Y. Wan, C. Sköld, M. Botros, M.-O. Guimond, A. Joshi, F. Nyberg, *J. Med. Chem.* **2012**, *55*, 2265–78.
[30] M.-O. Guimond, C. Wallinder, M. Alterman, A. Hallberg, N. Gallo-Payet, *Eur. J. Pharmacol.* **2013**, *699*, 160–171.
[31] H. Zhang, H. Unal, C. Gati, G. W. Han, W. Liu, N. A. Zatsepin, D. James, D. Wang, G. Nelson, U. Weierstall, *Cell* **2015**, *161*, 833–844.
[32] H. Zhang, H. Unal, R. Desnoyer, G. Won Han, N. Patel, V. Katritch, S. S. Karnik, V. Cherezov, R. C. Stevens, *J. Biol. Chem.* **2015**, *290*, 29127–29139.
[33] J. Sallander, C. Wallinder, A. Hallberg, J. Åqvist, H. Gutiérrez-De-Terán, *Bioorg. Med. Chem. Lett.* **2016**, *26*, 1355–1359.
[34] H. Zhang, G. W. Han, A. Batyuk, A. Ishchenko, K. L. White, N. Patel, A. Sadybekov, B. Zamlynny, M. T. Rudd, K. Hollenstein, *Nature* **2017**, *544*, 327–332.
[35] J. Wannberg, R. Isaksson, U. Bremberg, M. Backlund, J. Sävmarker, M. Hallberg, M. Larhed, *Bioorg. Med. Chem. Lett.* **2018**, *28*, 519–522.
[36] D. Nöteberg, W. Schaal, E. Hamelink, L. Vrang, M. Larhed, *J. Comb. Chem.* **2003**, *5*, 456–464.
[37] M. Larhed, A. Hallberg, *Drug Discovery Today* **2001**, *6*, 406–416.
[38] L. G. Ulysse, Q. Yang, M. D. Mclaws, D. K. Keefe, P. R. Guzzo, B. P. Haney, *Org. Process Res. Dev.* **2010**, *14*, 225–228.
[39] P. E. Eaton, G. R. Carlson, J. T. Lee, *J. Org. Chem.* **1973**, *38*, 4071–4073.
[40] J. A. Ballesteros, H. Weinstein, in *Methods Neurosci.* Academic Press, **1995**, pp. 366–428.
[41] B. K. Park, N. R. Kitteringham, P. M. O'neill, *Annu. Rev. Pharmacol. Toxicol.* **2001**, *41*, 443–70.
[42] K. Müller, C. Faeh, F. Diederich, *Science* **2007**, *317*, 1881–6.
[43] N. J. Kevin, R. A. Rivero, W. J. Greenlee, R. S. L. Chang, T. B. Chen, *Bioorg. Med. Chem. Lett.* **1994**, *4*, 189–194.
[44] M.-O. Guimond, M. Hallberg, N. Gallo-Payet, C. Wallinder, *ACS Med. Chem. Lett.* **2014**, *5*, 1129–1132.
[45] E. S. Jones, M. P. Del Borgo, J. F. Kirsch, D. Clayton, S. Bosnyak, I. Welungoda, N. Hausler, S. Unabia, P. Perlmutter, W. G. Thomas, *Hypertension* **2011**, *57*, 570–576.
[46] S. Bosnyak, E. S. Jones, A. Christopoulos, M.-I. Aguilar, W. G. Thomas, R. E. Widdop, *Clin. Sci.* **2011**, *121*, 297–303.
[47] M. Del Borgo, Y. Wang, S. Bosnyak, M. Khan, P. Walters, I. Spizzo, P. Perlmutter, L. Hilliard, K. Denton, M.-I. Aguilar, *Clin. Sci.* **2015**, *129*, 505–513.
[48] J. B. Houston, *Biochem. Pharmacol.* **1994**, *47*, 1469–1479.
[49] R. S. Obach, *Drug Metab. Dispos.* **1999**, *27*, 1350–1359.
[50] R. A. Friesner, J. L. Banks, R. B. Murphy, T. A. Halgren, J. J. Klicic, D. T. Mainz, M. P. Repasky, E. H. Knoll, M. Shelley, J. K. Perry, *J. Med. Chem.* **2004**, *47*, 1739–1749.
[51] T. A. Halgren, R. B. Murphy, R. A. Friesner, H. S. Beard, L. L. Frye, W. T. Pollard, J. L. Banks, *J. Med. Chem.* **2004**, *47*, 1750–1759.
[52] R. A. Friesner, R. B. Murphy, M. P. Repasky, L. L. Frye, J. R. Greenwood, T. A. Halgren, P. C. Sanschagrin, D. T. Mainz, *J. Med. Chem.* **2006**, *49*, 6177–6196.
[53] H. Gutiérrez-de-Terán, X. Bello, D. Rodríguez, *Biochem. Soc. Trans.* **2013**, *41*, 205–212.
[54] M. Esguerra, A. Siretskiy, X. Bello, J. Sallander, H. Gutiérrez-de-Terán, *Nucleic Acids Res.* **2016**, *44*, W455–W462.
[55] B. Hess, C. Kutzner, D. Van Der Spoel, E. Lindahl, *J. Chem. Theory Comput.* **2008**, *4*, 435–447.
[56] G. A. Kaminski, R. A. Friesner, J. Tirado-Rives, W. L. Jorgensen, *J. Phys. Chem. B* **2001**, *105*, 6474–6487.
[57] O. Berger, O. Edholm, F. Jähnig, *Biophys. J.* **1997**, *72*, 2002–2013.
[58] A. J. Venkatakrishnan, X. Deupi, G. Lebon, C. G. Tate, G. F. Schertler, M. Madan Babu, *Nature* **2013**, *494*, 185–194.

Manuscript received: December 6, 2018
Revised manuscript received: January 2, 2019
Version of record online: ■■, ■■■